ACS APPLIED NANO MATERIALS

www.acsanm.org Article

High-Sensitivity Low-Energy Ion Spectroscopy with Sub-Nanometer Depth Resolution Reveals Oxidation Resistance of MoS_2 Increases with Film Density and Shear-Induced Nanostructural Modifications of the Surface

Tomas F. Babuska, John F. Curry, Ryan Thorpe, Md. Istiaque Chowdhury, Nicholas C. Strandwitz, and Brandon A. Krick*

Cite This: *ACS Appl. Nano Mater.* 2023, 6, 1153−1160 Read Online

ACCESS | Metrics & More | Article Recommendations

ABSTRACT: For decades, density has been attributed as a critical aspect of the structure of sputter-deposited nanocrystalline molybdenum disulfide (MoS_2) coatings impacting oxidation resistance and wear resistance. Despite its importance, there are few examples in the literature that explicitly investigate the relationship between the density and oxidation behaviors of MoS_2 coatings. Aging and oxidation are primary considerations for the use of MoS_2 coatings in aerospace applications as they inevitably experience prolonged storage in water and oxygen-rich environments prior to use. Oxidation that is either limited to the first few nanometers or through the bulk of the coating can result in seizure due to high initial coefficients of friction or component failure from excessive wear. High-sensitivity low-energy ion spectroscopy (HS-LEIS) and Rutherford backscattering spectrometry (RBS) are both used to understand the extent of oxidation throughout the first ∼10 nanometers of the surface of pure sputtered nanocrystalline MoS_2 coatings after high-temperature aging and how it is impacted by the density of coatings as measured by RBS. Results show that low-density coatings (ρ = 3.55 g/cm^3) exhibit a more columnar microstructure and voiding, which act as pathways for oxidative species to penetrate and interact with edge sites, causing severe surface and subsurface oxidation. Furthermore, HS-LEIS of surfaces sheared prior to oxidation reveals that the oxidation resistance of low-density MoS_2 coatings can be significantly improved by shear-induced reorientation of the surface microstructure to a basal orientation and elimination of pathways for oxygen into the bulk through compaction of surface and subsurface voids.

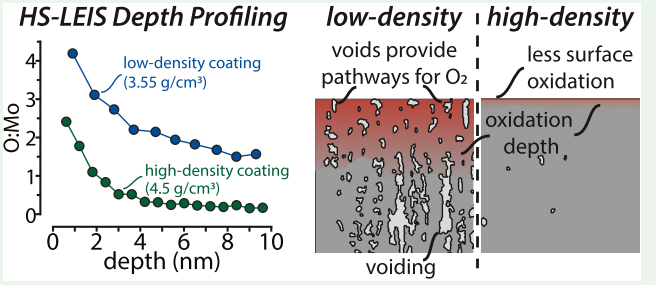

KEYWORDS: *high-sensitivity low-energy ion spectroscopy, low-density, direct current, high-density, focused ion beam, Rutherford backscattering spectrometry*

1. INTRODUCTION

Nanocrystalline sputter-deposited molybdenum disulfide (MoS_2) coatings are used as solid lubricants for space applications,[1] yet susceptibility to oxidation during prolonged periods of exposure to oxygen and water (i.e., aging) occurring in operating environments (such as preflight testing and component verification) can decrease the life of the coating and risk failure of hardware.[2] Oxidation is known to cause high initial friction, prolonged cycles to achieve steady-state friction (i.e., run-in), and premature failure[3] due to oxidative etching of MoS_2 to MoO_3[3,4] inhibiting the formation of low-shear-strength nanometer-thick basally oriented surface films.

The environmental resilience of MoS_2, from both aging during storage and atomic oxygen in low-earth orbit, is dependent on the orientation of the MoS_2 crystallites in the coating.[3,5−7] In this manuscript, a crystallite refers to the domain of contiguous individual lamella that are bound to one another by van der Waals interactions and in the same crystallographic orientation. Microstructures consisting of large, basally oriented crystallites limit the severity of surface oxidation and block oxidative species from penetrating and oxidizing the bulk coating.[7] Benefits of basally oriented coating microstructures are highlighted by Curry et al.[7] using nitrogen-impinged coatings consisting of large, basally oriented

Received: October 27, 2022
Accepted: December 20, 2022
Published: January 11, 2023

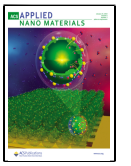

https://doi.org/10.1021/acsanm.2c04703
ACS Appl. Nano Mater. 2023, 6, 1153−1160

crystallites capable of achieving steady-state coefficients of friction within fewer sliding cycles than sputter-deposited coatings. Often, sputter-deposited pure MoS_2 coatings are composed of either nanometer-sized crystallites with a vertical orientation (i.e., columnar) or are amorphous,[8−10] making them susceptible to oxidation.[3,7] When mechanical shear is applied through sliding, surface crystallites reorient to a ∼5−20 nanometer-thick basal orientation[11,12] and coalesce,[13] forming a low-shear-strength interface. The oriented surface layer composed of larger, basally oriented crystallites has been shown to improve the environmental resilience from water and oxygen over the as-deposited coating microstructure[14] and minimize unwanted increases in the initial coefficient of friction and prolonged run-in imparted by aging.

Coating composition can be modified using dopants, such as Ti, Ni, Sb_2O_3, and Au, improving aging resistance[15] and oxidation from atomic oxygen[16−18] due to densification of the coating. Densification of coatings with dopants, like titanium[19] or Sb_2O_3/Au,[20] increases the hardness and improves wear rates in humid environments. Dopants can impart further improvements by stabilizing the sliding interface through shear-induced coarsening of nanometer-sized filler particles below the surface, providing two key benefits: first, coarsened regions of dopants act as wells that supply MoS_2 to the surface[21] and second, minimize bulk interactions with water and oxygen by limiting diffusion into the coating.[22]

Correlations between coating microstructure and density for pure MoS_2 coatings have been observed by Buck,[23] with columnar (ρ = 3.8 ± 0.35 g/cm^3) and amorphous (ρ = 3.3 ± 0.35 g/cm^3) coatings being less dense than basally oriented coatings (ρ = 3.95 ± 0.35 g/cm^3). The decrease in density for columnar coatings has been attributed to the formation of nanometer-sized gaps between crystallites due to dendritic growth, while amorphous microstructures can exhibit lower densities due to a high degree of disorder and voiding. The cause for these voids is typically due to higher vertical growth rates of MoS_2 crystallites during sputter deposition than horizontal growth rates, resulting in fibrous columnar structures that shadow one another and lead to these features and more porous films.[24] Bolster et al.[25] used ion beam-assisted deposition (IBAD) to limit the vertical growth rate, allowing for highly dense pure MoS_2 coatings (ρ = 4.4 g/cm^3). Sources of contaminants, such as water on the substrate surface or in the plasma, during deposition, promote the nucleation of columnar microstructures[26] and, in cases of high-water content, cause amorphization and high oxygen content in the film.[27] Lince[26] observed that oxygen (predominantly from H_2O in the deposition chamber) will substitute sulfur in the lattice of MoS_2, forming $MoS_{2-x}O_x$ films and has a major effect on their resulting crystallinity, structure, and morphology. With increasing oxygen content, $MoS_{2-x}O_x$ films can have lower wear rates than pure MoS_2 due to oxygen-mediated crystallite size reduction densifying the coating.[28] Though densification from oxygen improves wear life, substitutional oxygen can make coatings susceptible to environmental species by providing sites for water to interact at basal surfaces, causing hydrogen bonding that leads to increases in coefficient of friction, wear rate, and oxidation.[29]

While density has been a key attribute driving both the tribological performance and aging resistance of sputter-deposited MoS_2 coatings, explicit measurements of density and its role in oxidation are lacking. As previous works have focused on relationships between oxidation and crystallite orientation[7,14] or oxidation and composition,[15] this work aims to solidify the density−oxidation relationship using Rutherford backscattering spectroscopy (RBS) to quantify coating density and high-sensitivity low-energy ion spectroscopy (HS-LEIS) to probe oxidation of the first few nanometers after accelerated aging experiments after high-temperature oxygen exposures.

2. EXPERIMENTAL METHODS

2.1. Materials Synthesis. *2.1.1. Deposition of the Low-Density (LD) Coating.* Radio frequency (RF) magnetron sputtering with a target power of 120 W was used to deposit pure MoS_2 films in a vacuum deposition system with a base pressure of 5 × 10^{-6} torr. Direct current (DC) magnetron sputtering with a target power of 80 W was used to deposit a 99.99% pure titanium adhesion layer (∼100 nm thick) onto substrates made of 440C steel (∼20 nm R_a roughness). Substrates were fixed to a rotating stage with a 50 VDC bias. After sputtering the Ti adhesion layer, a ∼200 nm gradient layer of Ti/MoS_2 was deposited, followed by an ∼800 nm thick pure MoS_2 coating for 2.5 h (∼1.27 Å/s).

2.1.2. Deposition of the High-Density (HD) Coating. Arc evaporation was used to deposit an ∼10 nm Cr adhesion layer onto polished 440C steel substrates (∼20 nm R_a roughness) prior to the deposition of the MoS_2 coating. DC magnetron sputtering with a target power of 150 W on a 3″ target, 1.5 mTorr Ar, and a 30 VDC bias for 30 min was used to deposit 1 μm thick pure MoS_2 coatings (∼5.55 Å/s).

2.2. Focused Ion Beam (FIB)/Transmission Electron Microscopy (TEM). A Dualbeam Thermo Fisher Helios focused ion beam (FIB) was used to prepare the cross section of the low-density (LD) and high-density (HD) coatings. A protective Pt layer (∼2 μm) was deposited by first using the electron beam, followed by the ion beam. Cross sections of LD were studied with a transmission electron microscope (TEM) (JEOL JEM-ARM200cF, Tokyo, Japan) at 200 kV using scanning TEM (STEM) dark-field and bright-field imaging. Cross sections of HD were studied using high-angle annular dark-field (HAADF) imaging in an aberration-corrected scanning TEM (FEI Titan G2 80-200 STEM) operated at 200 kV.

2.3. X-ray Diffraction (XRD). X-ray diffraction (XRD) measurements were acquired with a PANalytical Empyrean diffractometer using a Cu X-ray tube with a wavelength of 1.541 Å. The incident beam was shaped with a Bragg-Brentano HD mirror, and slits were used to maximize the irradiation on the sample. A 7.5 mm antiscatter slit and a Soller slit were used to shape the diffracted beam, which was detected with a PIXcel3D-Medipix3 1 × 1 area detector in scanning line 1D mode. A step size of 0.0066° and a counting rate of 25 s/step were used to take symmetric θ−2θ (gonio) scans.

2.4. Accelerated Aging and High-Sensitivity Low-Energy Ion Spectroscopy (HS-LEIS). Accelerated aging (Scheme 1) was performed in the antechamber of the HS-LEIS by heating the samples to 250 °C for 30 min under 1 mbar O_2 or to 250 °C for 12 h under 10 mbar O_2. After oxidation, samples were transferred directly from the antechamber into the analysis chamber to avoid any exposure to atmosphere. Spectra were acquired using an ION-TOF Qtac^{100} HS-

Scheme 1. Oxidation of MoS_2 under Accelerated Aging Conditions

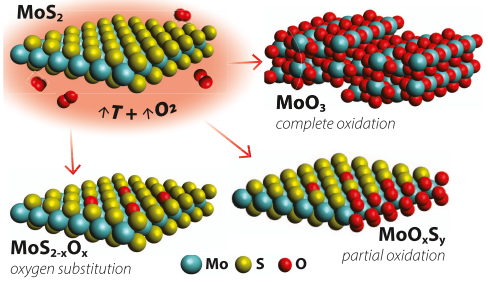

https://doi.org/10.1021/acsanm.2c04703
ACS Appl. Nano Mater. 2023, 6, 1153−1160

LEIS instrument. The analysis beam was 3 keV He^+ rastered over an area of 1 × 1 mm, and the sputter beam was 0.5 keV Ar^+ rastered over an area of 2 × 2 mm. Depth profiles removed ~1 nm of material per cycle with a final depth of ~20 nm. Charge neutralization using a beam of low-energy electrons was used during the measurements to keep the surface of the sample grounded. The toroidal analyzer was operated at a pass energy of 3000 V. Peak intensities were determined using linear background subtraction and were normalized to the beam dose. Elemental sensitivity factors were measured empirically using reference samples with known stoichiometries.

2.5. Rutherford Backscattering Spectrometry (RBS). Infinita Laboratories, Saratoga, CA, performed Rutherford backscatter spectrometry (RBS). A 1.9 MeV $4He^+$ beam with detection at a 165° scattering angle and an average beam current of 5 nA with an integrated charge of 2.0 μC was used for RBS. The spot size of the RBS had a diameter of ~10 mm (78.5 mm^2 analysis area). Areal densities (N_{af}) were calculated by fitting the spectra using SIMNRA,[30] and coating thickness (t) was measured from TEM. Coating density (ρ) was calculated using eq 1, where (M) is the molar mass of MoS_2 and (N_a) is Avogadro's number multiplied by the number of atoms in a unit cell (three for MoS_2). Though both coatings were measured with RBS to be sub-stoichiometric, with HD and LD having S/Mo ratios of 1.94 and 1.6, respectively, density was calculated under the assumption of stoichiometric MoS_2.

$$\rho = \frac{N_{af}{}^{*}M}{t^{*}N_a} \quad (1)$$

The coating oxygen content of LD and HD was measured with Rutherford backscattering spectrometry (RBS) to decouple bulk oxygen from the oxygen introduced from aging and showed that both films have oxygen contents below 5 atom %.

2.6. Shear-Modified Surface Regions. The basally oriented surfaces of MoS_2 used in the oxidation studies were prepared by sliding a 3 mm diameter spherical probe against the coatings. As the HS-LEIS analysis regions (1 mm × 1 mm) are significantly larger than a wear scar (~10 to 50 μm wide), we created a 5 mm × 5 mm shear-modified region. These large "shear-modified" areas were created by rastering a steel probe in a 5 mm × 5 mm region using a tribometer as previously done by Babuska et al.[14] The probe was loaded against the coated sample with a normal force, F_N = 200 mN. Twenty bidirectional sliding cycles are performed in a single location before rastering in 10 μm increments. A total of 10,000 sliding cycles are done on each shear-modified region.

3. RESULTS AND DISCUSSION

Transmission electron micrographs (TEM) of the low-density (LD) and high-density (HD) pure nanocrystalline MoS_2 coatings show the formation of voids throughout the thickness of LD corresponding to a low measured density of 3.55 g/cm^3 (Figure 1a). The theoretical density for MoS_2 has been reported to vary between 4.8 and 5.06 g/cm^3,[25,31,25,31] above the measured density of HD (ρ = 4.5 g/cm^3). X-ray diffraction (XRD) of LD and HD (Figure 1b) shows two different coating morphologies (orientation and crystallinity), with LD consisting of less crystalline, vertically oriented crystallites (i.e., columnar) indicated by a low-intensity peak at 33.2° correlating to the $(10\bar{1}0)$ plane of hexagonal crystal structure (ICDD 01-077-1716). HD has higher intensity peaks at 12.7, 33.2, and 59.5° corresponding to (0002), $(10\bar{1}0)$, and $(11\bar{2}0)$ planes, indicative of a randomly oriented nanocrystalline coating (Figure 1b). The shift of the (0002) peak to 12.7° from 14.3° for HD and of the $(10\bar{1}0)$ peak to 33.2° for LD has been shown to occur for sputter-deposited coatings due to lattice expansion caused by oxygen impurities.[10] The correlation between columnar microstructures and the formation of voids is a result of high vertical growth rates

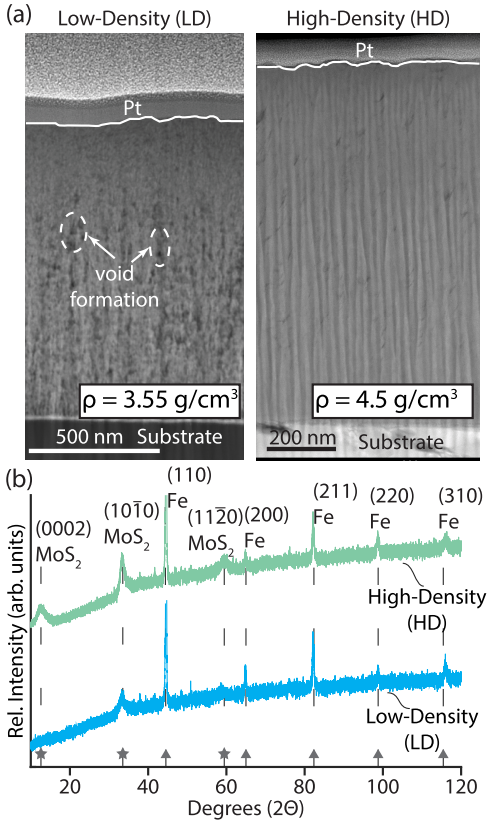

Figure 1. Transmission electron microscopy (TEM) of the low-density (LD) and high-density (HD) coatings showing voids in LD, resulting in a low measured film density of 3.55 g/cm^3 compared to 4.5 g/cm^3 for HD (a). X-ray diffraction (XRD) of LD and HD (b) indicates that LD is preferentially $(10\bar{1}0)$ oriented (i.e., columnar), whereas HD has peaks relating to (0002), $(10\bar{1}0)$, and $(11\bar{2}0)$ planes (i.e., randomly oriented).

and low horizontal growth of MoS_2 crystallites during deposition, resulting in edge-oriented crystallites shadowing incoming deposits from the surface, causing pores.[24]

Results of the raw HS-LEIS spectra of the 12 h O_2 aged samples are shown in Figure 2. The impact of voids (i.e., density) and coating orientation (randomly oriented vs columnar) on the oxidation resistance of sputter-deposited MoS_2 coatings due to accelerated aging is shown by HS-LEIS depth profiles of LD and HD after high-temperature oxygen exposures (Figure 2a,b). We observe a pronounced O peak at 1150 eV throughout the sputtered depth (~10 nm) of LD after the 12 h (Figure 2a) oxygen exposure, indicating surface and subsurface oxidation. The O peak for the higher density coating (HD) after the 12 h (Figure 2b) exposure reveals mild surface oxidation indicated by weak peak intensities near the surface (~1 nm) that subsequently decreases in intensity through the sputtered depth. The main source of background intensity in HS-LEIS is scattering from subsurface layers.[32] The background intensity in the 600−1000 eV range is typically associated with hydrocarbons.[32] Denser and thicker coatings typically result in higher background intensities,[32] as is the case with the high-density MoS_2 coating in Figure 2b. We observe a peak correlating to Na only for the high-density coating (Figure 2b,d), which we attribute to surface contaminants such as Na_2O. While Na was unexpected, we do not believe it impacts the behavior as it is removed via sputtering in the first

https://doi.org/10.1021/acsanm.2c04703
ACS Appl. Nano Mater. 2023, 6, 1153−1160

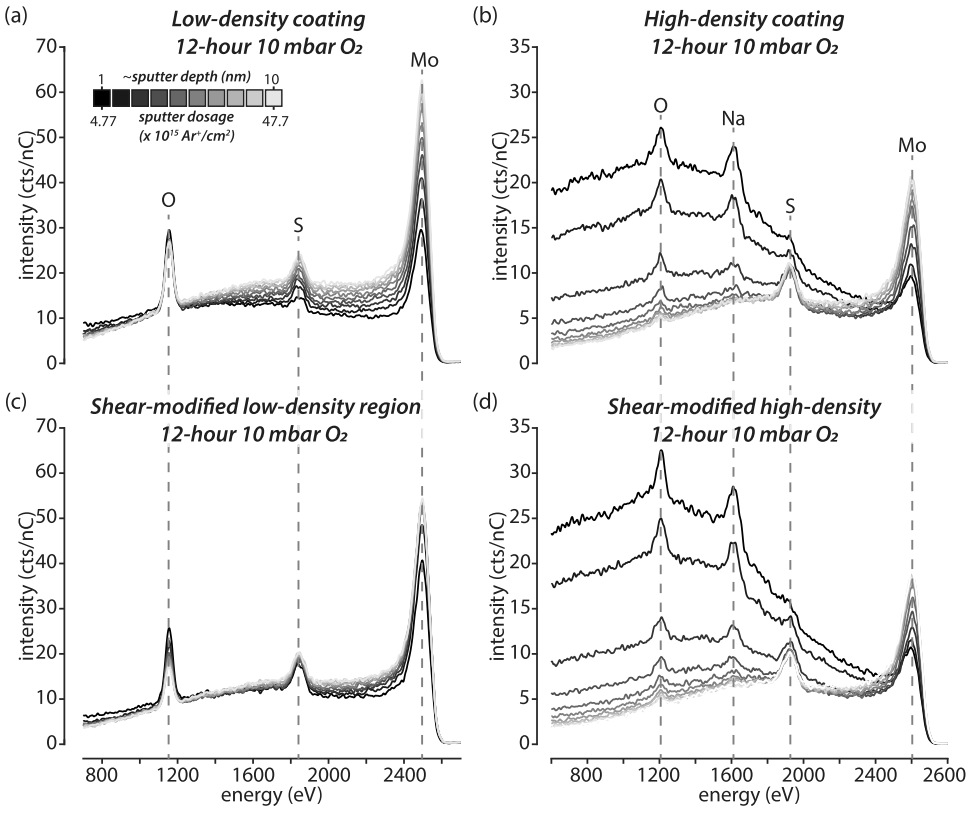

Figure 2. HS-LEIS spectra showing peaks for O (1150 eV), S (1820 eV), and Mo (2500 eV) as a function of sputter depth for each sample and aging condition studied. (a) Low-density (LD) coating after 12 h of 10 mbar 250 °C O_2. (b) High-density (HD) coating after 12 h of 10 mbar 250 °C O_2. (c) Shear-modified region of the low-density coating. (d) Shear-modified region of the high-density coating after 12 h 10 mbar 250 °C O_2 Note: there is a shift in the energies between (a/c) and (b/d) due to a change in the calibration of the beam energy of the HS-LEIS. (a and c) have a beam energy of 3 kV, whereas (b and d) have a beam energy of 3.1 kV.

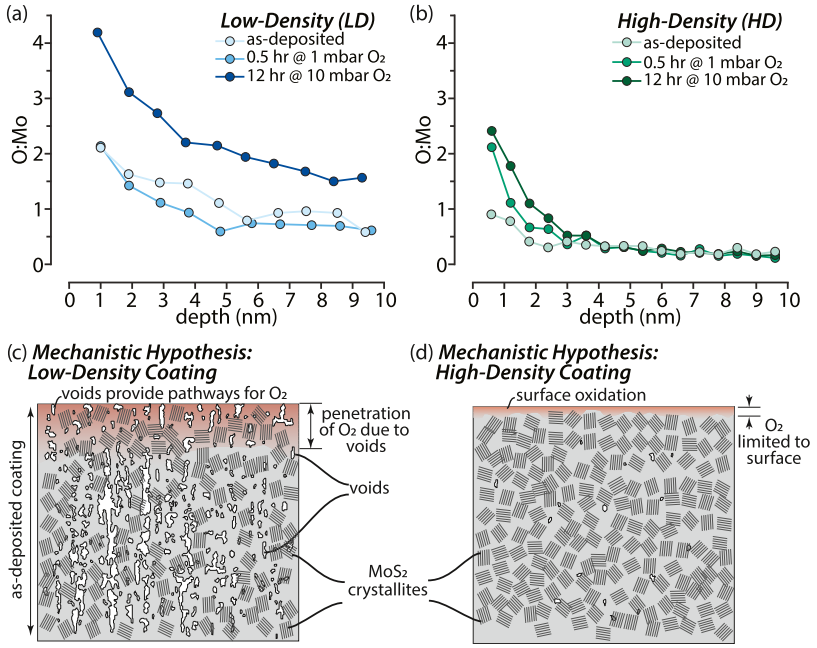

Figure 3. Ratio of oxygen to molybdenum (O/Mo) as a function of sputter depth measured using depth profiling HS-LEIS for the as-deposited (a) low-density (LD) and (b) high-density (HD) coatings for unaged as well as aged samples at 250 °C of 1 mbar O_2 for 0.5 h and at 250 °C of 10 mbar O_2 for 12 h. (c, d) Mechanistic hypothesis describing the role of density on the oxidation behavior of pure MoS_2 coatings is presented for (c) low-density and (d) high-density coatings. (c) Low-density coatings allow oxygen to penetrate a coating and cause severe oxidation of the coating. (d) Oxidation is limited to the surface of high-density coatings by minimizing penetration pathways.

https://doi.org/10.1021/acsanm.2c04703
ACS Appl. Nano Mater. 2023, 6, 1153−1160

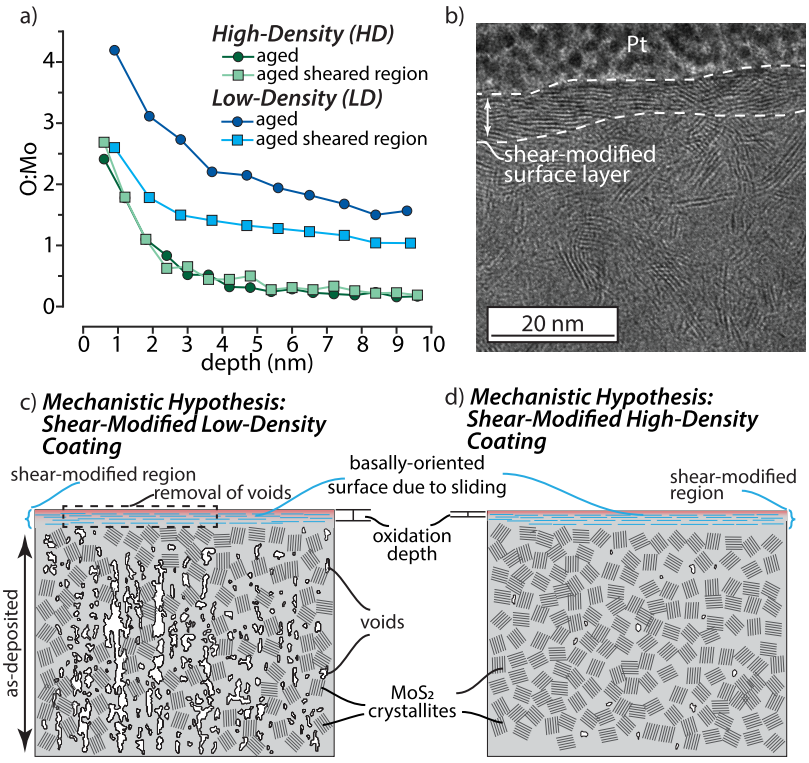

Figure 4. (a) Ratio of oxygen to molybdenum (O/Mo) as a function of sputter depth measured using depth profiling HS-LEIS comparing shear-modified and nonshear-modified low-density (LD) and high-density (HD) coatings after aging experiments at 250 °C of 10 mbar O_2 for 12 h. (b) High-resolution transmission electron micrograph showing the basally oriented surface of the shear-modified layer in low-density coatings before aging. (c, d) Mechanistic hypothesis describing the role of density on the oxidation behavior of shear-modified MoS_2 coatings is presented for (c) low-density and (d) high-density coatings. (c) For low-density coatings, sliding imparts additional improvements by compacting voids near the surface and densifying the subsurface of the coating. (d) Oxidation is limited to the surface of high-density coatings by minimizing penetration pathways. In both cases, sliding causes reorientation of MoS_2 crystallites near the surface to become basally oriented, which further limits oxidation due to less-reactive sulfur planes as opposed to more reactive edge sites, preventing sites for oxygen to bond and blocking pathways into the film.

4 nm and is commonly observed on a variety of surfaces measured by HS-LEIS.

The differences in oxidation resistance between high- and low-density coatings become more apparent when calculating the O/Mo ratios as a function of depth (Figure 3). It should be noted that sputtering can cause preferential removal of lighter elements such as sulfur and oxygen, resulting in potentially lower O/Mo ratios. The O/Mo ratio for LD after the 12 h oxygen exposure (O/Mo > 1.5 at 10 nm) is significantly higher than the as-deposited untreated coating (O/Mo < 1 at 10 nm) at all measured depths, whereas the depth profile for the 0.5 h oxygen exposure shows comparable O/Mo ratios as the as-deposited unoxidized low-density coating (Figure 3a). The O/Mo ratio as a function of depth for HD is lower (O/Mo < 0.5 at 10 nm; Figure 3b) than LD after both oxygen exposures though the surface (top 3 nm) of the high-density does show a mild increase in oxygen over the untreated as-deposited HD surface (O/Mo ∼ 1; Figure 3b).

Severe surface oxidation (O/Mo > 2) and penetration of oxygen into the subsurface (O/Mo > 1.5 at 10 nm) is attributed to both the columnar microstructure and porosity of the LD coating. It should be noted that a ratio of O/Mo greater than 3 (i.e., more oxygen than what would be found from MoO_3) is likely due to a combination of MoO_3 and surface-bound contaminants such as CO or Na_2O, as it is unlikely that the surface is MoO_4 because Mo cannot have an oxidation state of +8. Depth profiles exhibiting O/Mo ratios less than 3 could be due to multiple factors, including incomplete oxidation of MoS_2 resulting in molybdenum-oxysulfide, edges terminated with hydroxyl species, preferential sputtering of oxygen, or nonuniform oxidation of the surface creating regions of MoO_3 and MoS_2. X-ray photoelectron spectroscopy (XPS) of shear-modified MoS_2 surfaces by Babuska et al.[14] showed that the surface is composed of a mixture of MoS_2 and MoO_x (∼36%), equating to a O/Mo of 1.89.

Basally oriented coating microstructures composed of MoS_2 crystallite oriented parallel to the substrate have been shown by Curry et al.[7] and Fleischauer[3] to be more resistant to oxidation than amorphous and columnar coatings by limiting pathways for oxygen to penetrate into the coating and reducing the number of reactive edge sites where oxidation occurs. The columnar microstructure of the LD coating makes the surface susceptible to severe oxidation from environmental water and oxygen by exposing unterminated basal plane edges to the environment. This is supported by results from HS-LEIS showing a high measured surface O/Mo ratio (top 1 nm) for LD after the 12 h, 10 mbar oxygen exposure. Though the LD sample is more susceptible to oxidation, we observe relatively no change in the top surface oxygen content after the 0.5 h, 1 mbar oxygen exposure from that of the untreated as-deposited surface (Figure 3a). At depths of 2−5 nm, the O/Mo ratio is slightly lower after the 0.5 h, 1 mbar oxygen exposure than for the as-deposited coating. We attribute this difference to the removal of physisorbed oxygen-containing species from the porous surface and subsurface, such as hydrocarbons or water,

https://doi.org/10.1021/acsanm.2c04703
ACS Appl. Nano Mater. 2023, 6, 1153−1160

due to elevated temperatures in a vacuum atmosphere the sample is exposed to during the mild oxygen treatment. HS-LEIS of the as-deposited LD coating surface (Figure 3a) indicates that the surface is already composed of significant oxide (O/Mo > 2) before any oxygen exposure is performed. The formation of a preexisting surface oxide eliminates potential edge sites imparted by the columnar microstructure as they are already oxidized. Further oxidation and growth of the surface oxide require exposure to more oxygen for longer durations (i.e., 12 h at 10 mbar O_2). For the HD coating, we observe that the 0.5 h exposure increases the amount of surface oxide over the as-deposited coating due to the lack of a well-formed preexisting surface oxide (Figure 3b), resulting in any available edge sites becoming oxidized. Once any available surface edge sites have been terminated, the dense and nanocrystalline nature of HD helps block the penetration of oxygen. In turn, this limits the growth of any oxide into the coating, as indicated by HS-LEIS after the 12 h, 10 mbar O_2 exposure (Figure 3b).

A mechanistic hypothesis describing the oxidation of porous coatings is shown in Figure 3c. The presence of voids (1) provides pathways for oxygen to penetrate the coating, causing subsurface oxidation (Figure 3c), and (2) exposes additional edge sites within the coating, increasing the susceptibility to oxidation. Additionally, a deficiency in sulfur causing sub-stoichiometric MoS_2 (S/Mo = 1.6 for LD coatings) provides further defect sites for oxidation. We observe the resulting oxidation behavior of a porous columnar film in the depth profile of the LD coating (Figure 3a) with elevated ratios of O/Mo throughout the top 10 nm. Highly dense, randomly oriented near-stochiometric (S/Mo = 1.94) coatings, such as HD, limit the severity of (1) surface oxidation by minimizing reactive edge sites through changes in orientation expressing less-reactive basal surfaces and (2) bulk oxidation from the absence pathways from voids (Figure 3d). The superior resistance to oxidation imparted by increased density and crystallinity for HD is highlighted by the mild surface oxidation (O/Mo ~ 2.5) and a low subsurface oxygen content (O/Mo < 0.5) measured after ~5 nm of sputtering regardless of oxygen exposure time or concentration.

In applications that require prolonged storage in the presence of water/oxygen, even coatings with unfavorable morphology, such as low coating densities or columnar microstructures, can be modified with mechanical shear to alter the surface microstructure to improve environmental resilience.[14] MoS_2 crystallites near the surface reorient under shear to a basal orientation[11,33] and coalesce into larger, less defective crystallites[13] with a lower shear strength, resulting in a low coefficient of friction. Babuska et al.[14] showed that sheared pure MoS_2 surfaces formed by sliding in dry N_2 or humid lab air result in basally oriented surface microstructures that decrease the initial coefficient of friction and sliding cycles required to reach steady-state friction before and after accelerated aging.

In this study, we investigated the improvements sheared surfaces have on the oxidation resistance of low-density coatings using the methods of creating large, shear-modified areas from Babuska et al.[14] While the HS-LEIS spectra of the 12 h oxygen aged, sheared HD surface (Figure 2d) are similar to aged, nonsheared coating (Figure 2b), indicating no significant improvements in oxidation resilience with sliding, the O peak of the aged and sheared LD surface (Figure 2c) decreases in intensity with sputtering to values below the nonsheared LD coating (Figure 2a). The O/Mo ratio as a function of depth for the aged sheared region of the LD coating (Figure 4a) shows a significant decrease in both the amount of surface oxidation (O/Mo ~ 2.5) and oxygen throughout the top 10 nm than the aged, nonsheared LD coating (Figure 3c), highlighting the importance shear has for improving the environmental resilience of low-density coatings (Figure 4c).

The degree to which shear-modifying the surface improves oxidation resistance depends on the initial coating morphology. HS-LEIS shows that for the 12 h, 250 °C 10 mbar oxygen treatment, the aging behavior of high-density coating is unaffected by the formation of a basally oriented surface (Figure 4a). It should be noted that in previous studies by Babuska et al.,[14] accelerated aging experiments had 20× more oxygen than the current study and the presence of water, a constituent known to accelerate the oxidation of MoS_2. Thus, in mild to moderate oxidative environments, HS-LEIS of the shear-modified and as-deposited HD surfaces suggests that density is the critical factor influencing the aging process over orientation due to the similarity in depth profiles for both regions. Sliding prior to aging is important for low-density coatings, which are highly susceptible to oxidation in their as-deposited state. Sliding on low-density coatings has two major roles, (1) it reorients the surface microstructure to be basally oriented (Figure 4b,c), thereby reducing potential edge sites for oxygen to bond, and (2) sliding densifies the coating by removing voids through compaction, eliminating pathways for oxygen to penetrate the coating (Figure 4c). Though we have not verified that sliding removes surface and subsurface voids in our coatings, Krauβ et al.[9] observed that highly porous pure MoS_2 coatings undergo compaction during sliding, the degree to which depends on sliding cycles and contact pressure. In the case of the high-density coatings, we posit that shear modification only reorients the film and does not densify it (Figure 4d); thus, the benefits of shear modification in mild oxidation conditions are not observed. We recommend sliding on the surface of MoS_2 coatings prior to aging and launch for applications, regardless of their density, for several reasons: (1) oxidation environments may be more extreme than those presented in the present work,[3,14,15] (2) run-in can reduce initial friction coefficients after long aging periods,[7,14] and (3) the variability in PVD processes can sometimes lead to coatings that are less dense or oriented differently than expected.

4. CONCLUSIONS

High-temperature oxygen exposures combined with HS-LEIS depth profiling of the top few nanometers were used to understand the role of coating density on the oxidation resistance of PVD-deposited pure nanocrystalline MoS_2 coatings. XRD and RBS showed that the two coatings studied were (1) a low-density (ρ = 3.55 g/cm^3) coating exhibiting a columnar microstructure with voiding and (2) a high-density (ρ = 4.5 g/cm^3) coating exhibiting a randomly oriented nanocrystalline microstructure. HS-LEIS showed that low-density coatings are susceptible to severe surface oxidation and bulk oxidation due to voids providing pathways into the coating and exposing reactive edge sites that promote oxidation. Sliding prior to oxidation was observed to impart no additional oxidation resistance for high-density coatings due to density driving oxidation resistance more than coating orientation when compared to low-density films. Identical HS-

https://doi.org/10.1021/acsanm.2c04703
ACS Appl. Nano Mater. 2023, 6, 1153−1160

LEIS depth profiles of the top 20 nm's on the sheared and as-deposited regions of the high-density coating suggest that in mild to moderately oxidative environments, density influences oxidation resistance more than orientation. The environmental resistance of low-density coatings was significantly improved by sliding prior to oxidation by removing reactive edge sites by forming a few-nanometer-thick basally oriented surface and removing pathways for oxygen through compaction of surface and subsurface voids.

AUTHOR INFORMATION

Corresponding Author

Brandon A. Krick − *FAMU-FSU College of Engineering, Florida State University, Tallahassee, Florida 32310, United States;* orcid.org/0000-0003-3191-5433; Email: bkrick@fsu.edu

Authors

Tomas F. Babuska − *FAMU-FSU College of Engineering, Florida State University, Tallahassee, Florida 32310, United States; Material, Physical and Chemical Sciences Center, Sandia National Laboratories, Albuquerque, New Mexico 87185-5820, United States; Mechanical Engineering Department, Lehigh University, Bethlehem, Pennsylvania 18015-3027, United States*

John F. Curry − *Material, Physical and Chemical Sciences Center, Sandia National Laboratories, Albuquerque, New Mexico 87185-5820, United States*

Ryan Thorpe − *Institute of Functional Materials and Devices, Lehigh University, Bethlehem, Pennsylvania 18015-3027, United States*

Md. Istiaque Chowdhury − *Materials Science and Engineering Department, Lehigh University, Bethlehem, Pennsylvania 18015-3027, United States;* orcid.org/0000-0002-1920-2978

Nicholas C. Strandwitz − *Materials Science and Engineering Department, Lehigh University, Bethlehem, Pennsylvania 18015-3027, United States*

Complete contact information is available at: https://pubs.acs.org/10.1021/acsanm.2c04703

Funding

This material is based upon work supported by the National Science Foundation under Grant Nos. 2027029, 1826251, and NSF GRFP No. 1842163. TEM work was performed at the National High Magnetic Field Laboratory, which is supported by National Science Foundation Cooperative Agreement No. DMR-1644779 and the State of Florida. This work was funded by the Laboratory Directed Research and Development (LDRD) program at Sandia National Laboratories, a multi-mission laboratory managed and operated by National Technology and Engineering Solutions of Sandia, LLC., a wholly owned subsidiary of Honeywell International, Inc., for the U.S. Department of Energy's National Nuclear Security Administration under contract DE-NA0003525. This paper describes objective technical results and analysis. Any subjective views or opinions that might be expressed in the paper do not necessarily represent the views of the U.S. Department of Energy or the United States Government.

Notes

The authors declare no competing financial interest.

ACKNOWLEDGMENTS

The authors would like to acknowledge Gary Doll for manufacturing coatings, Tomas Grejtak, Yan Xin, and Ping Lu for FIB/TEM, Filippo Mangolini, Mike Dugger, and Mike Chandross for thoughtful discussions on MoS_2.

REFERENCES

(1) Lince, J. R.; Loewenthal, S. H.; Clark, C. S. In *Degradation of Sputter-Deposited Nanocomposite MoS2 Coatings for NIRCam during Storage in Air*, Proceedings of the 43rd Aerospace Mechanisms Symposium, 2016.

(2) Krantz, T.; Hakun, C.; Cameron, Z.; Shareef, I.; Dube, M. In *Performance of MoS2 Coated Gears Exposed to Humid Air During Storage*, Proceedings of the 44th Aerospace Mechanisms Symposium, 2106.

(3) Fleischauer, P. D. Effects of Crystallite Orientation on Environmental Stability and Lubrication Properties of Sputtered MoS2 Thin Films. *ASLE Trans.* **1984**, *27*, 82−88.

(4) Walter, T. N.; Kwok, F.; Simchi, H.; Aldosari, H. M.; Mohney, S. E. Oxidation and Oxidative Vapor-Phase Etching of Few-Layer MoS2. *J. Vac. Sci. Technol., B* **2017**, *35*, No. 021203.

(5) Fleischauer, P. D. Fundamental Aspects of the Electronic Structure, Materials Properties and Lubrication Performance of Sputtered MoS2 Films. *Thin Solid Films* **1987**, *154*, 309−322.

(6) Curry, J. F.; Argibay, N.; Babuska, T.; Nation, B.; Martini, A.; Strandwitz, N. C.; Dugger, M. T.; Krick, B. A. Highly Oriented MoS2 Coatings: Tribology and Environmental Stability. *Tribol. Lett.* **2016**, *64*, 11.

(7) Curry, J. F.; Wilson, M. A.; Luftman, H. S.; Strandwitz, N. C.; Argibay, N.; Chandross, M.; Sidebottom, M. A.; Krick, B. A. Impact of Microstructure on MoS2 Oxidation and Friction. *ACS Appl. Mater. Interfaces* **2017**, *9*, 28019−28026.

(8) Zhang, R.; Cui, Q.; Weng, L.; Sun, J.; Hu, M.; Fu, Y.; Wang, D.; Jiang, D.; Gao, X. Modification of Structure and Wear Resistance of Closed-Field Unbalanced-Magnetron Sputtered MoS2 Film by Vacuum-Heat-Treatment. *Surf. Coat. Technol.* **2020**, *401*, No. 126215.

(9) Krauß, S.; Seynstahl, A.; Tremmel, S.; Meyer, B.; Bitzek, E.; Göken, M.; Yokosawa, T.; Zubiri, B. A.; Spiecker, E.; Merle, B. Structural Reorientation and Compaction of Porous MoS2 Coatings during Wear Testing. *Wear* **2022**, *500*−*501*, No. 204339.

(10) Lince, J. R.; Fleischauer, P. D. Crystallinity of Rf-Sputtered MoS2 Films. *J. Mater. Res.* **1987**, *2*, 827−838.

(11) Moser, J.; Levy, F. MoS_{2-x} Lubricating Films: Structure and Wear Mechanisms Investigated by Cross-Sectional Transmission Electron Microscopy. *Thin Solid Films* **1993**, *228*, 257−260.

(12) Hilton, M. R.; Bauer, R.; Fleischauer, P. D. Tribological Performance and Deformation of Sputter-Deposited MoS2 Solid Lubricant Films during Sliding Wear and Indentation Contact. *Thin Solid Films* **1990**, *188*, 219−236.

(13) Curry, J. F.; Ohta, T.; DelRio, F. W.; Mantos, P.; R Jones, M.; F Babuska, T.; Bobbitt, N. S.; Argibay, N.; A Krick, B.; Dugger, M. T.; Chandross, M. Structurally Driven Environmental Degradation of Friction in MoS2 Films. *Tribol. Lett.* **2021**, *69*, 96.

(14) Babuska, T. F.; Curry, J. F.; Dugger, M. T.; Lu, P.; Xin, Y.; Klueter, S.; Kozen, A. C.; Grejtak, T.; Krick, B. A. Role of Environment on the Shear-Induced Structural Evolution of MoS2 and Impact on Oxidation and Tribological Properties for Space Applications. *ACS Appl. Mater. Interfaces* **2022**, *14*, 13914−13924.

(15) Lince, J. R.; Loewenthal, S. H.; Clark, C. S. Tribological and Chemical Effects of Long Term Humid Air Exposure on Sputter-Deposited Nanocomposite MoS2 Coatings. *Wear* **2019**, *432*−*433*, No. 202935.

(16) Cross, J. B.; Martin, J. A.; Pope, L. E.; Koontz, S. L. Atomic Oxygen-MoS2 Chemical Interactions. *Surf. Coat. Technol.* **1990**, *42*, 41−48.

(17) Wang, P.; Qiao, L.; Xu, J.; Li, W.; Liu, W. Erosion Mechanism of MoS2-Based Films Exposed to Atomic Oxygen Environments. *ACS Appl. Mater. Interfaces* **2015**, *7*, 12943−12950.

(18) Gao, X.; Hu, M.; Fu, Y.; Wang, D.; Jiang, D.; Weng, L.; Liu, W.; Sun, J. MoS2-Sb2O3 Film Exhibiting Better Oxidation-Resistance in Atomic Oxygen Environment. *Mater. Lett.* **2018**, *219*, 212−215.
(19) Wang, X.; Xing, Y.; Ma, S.; Zhang, X.; Xu, K.; Teer, D. G. Microstructure and Mechanical Properties of MoS2/Titanium Composite Coatings with Different Titanium Content. *Surf. Coat. Technol.* **2007**, *201*, 5290−5293.
(20) Scharf, T. W.; Kotula, P. G.; Prasad, S. V. Friction and Wear Mechanisms in MoS2/Sb2O3/Au Nanocomposite Coatings. *Acta Mater.* **2010**, *58*, 4100−4109.
(21) Zabinski, J. S.; Bultman, J. E.; Sanders, J. H.; Hu, J. J. Multi-Environmental Lubrication Performance and Lubrication Mechanism of MoS2/Sb2O3/C Composite Films. *Tribol. Lett.* **2006**, *23*, 155−163.
(22) Zabinski, J. S.; Donely, M. S.; McDevitt, N. T. Mechanistic Study of the Synergism between Sb203 and MoS2 Lubricant Systems Using Raman Spectroscopy. *Wear* **1993**, 103−108.
(23) Buck, V. Structure and Density of Sputtered MoS2 Films. *Vacuum* **1986**, *36*, 89−94.
(24) Seynstahl, A.; Krauß, S.; Bitzek, E.; Meyer, B.; Merle, B.; Tremmel, S. Microstructure, Mechanical Properties and Tribological Behavior of Magnetron-Sputtered MoS2 Solid Lubricant Coatings Deposited under Industrial Conditions. *Coatings* **2021**, *11*, No. 455.
(25) Bolster, R. N.; Singer, I. L.; Wegand, J. C.; Fayeulle, S.; Gossett, C. R. Preparation by Ion-Beam-Assisted Deposition, Analysis and Tribological Behavior of MoS2 Films. *Surf. Coat. Technol.* **1991**, *46*, 207−216.
(26) Lince, J. R. $MoS_{2-x}O_x$ Solid Solutions in Thin Films Produced by Rf-Sputter-Deposition. *J. Mater. Res.* **1990**, *5*, 218−222.
(27) Buck, V. Preparation and Properties of Different Types of Sputtered MoS2 Films. *Wear* **1987**, *114*, 264−274.
(28) Lince, J. R.; Hilton, M. R.; Bommannavar, A. S. Oxygen Substitution in Sputter-Deposited MoS2 Films Studied by Extended X-Ray Absorption Fine Structure, X-Ray Photoelectron Spectroscopy and X-Ray Diffraction. *Surf. Coat. Technol.* **1990**, *43*−*44*, 640−651.
(29) Fleischauer, P. D.; Lince, J. R. A Comparison of Oxidation and Oxygen Substitution in MoS2 Solid Film Lubricants. *Tribol. Int.* **1999**, *32*, 627−636.
(30) Mayer, M. SIMNRA, a Simulation Program for the Analysis of NRA, RBS and ERDA. *AIP Conf. Proc.* **1999**, *475*, 541−544.
(31) Haynes, W. M.*CRC Handbook of Chemistry and Physics*, 92nd ed.; CRC Press: Hoboken, 2011.
(32) Brongersma, H. H.; Draxler, M.; de Ridder, M.; Bauer, P. Surface Composition Analysis by Low-Energy Ion Scattering. *Surf. Sci. Rep.* **2007**, *62*, 63−109.
(33) Martin, J. M.; Pascal, H.; Donnet, C.; Mogne, T. L.; Le Mogne, T.; Loubet, J. L.; Loubet, J.; Epicier, T. Superlubricity of MoS2: Crystal Orientation Mechanisms. *Surf. Coat. Technol.* **1994**, *68*−*69*, 427−432.

https://doi.org/10.1021/acsanm.2c04703
ACS Appl. Nano Mater. 2023, 6, 1153−1160